



Evaluation of Permeability Models for Foundry Molds and Cores in Sand Casting Processes

D. Sundaram * , T. Matsushita , I. Belov, A. Diószegi 

School of Engineering, Jönköping University, Sweden

* Corresponding author: E-mail address: dinesh.sundaram@ju.se

Received 07.12.2023; accepted in revised form 06.02.2024; available online 18.03.2024

Abstract

Predicting the permeability of different regions of foundry cores and molds with complex geometries will help control the regional outgassing, enabling better defect prediction in castings. In this work, foundry cores prepared with different bulk properties were characterized using X-ray microtomography, and the obtained images were analyzed to study all relevant grain and pore parameters, including but not limited to the specific surface area, specific internal volume, and tortuosity. The obtained microstructural parameters were incorporated into prevalent models used to predict the fluid flow through porous media, and their accuracy is compared with respect to experimentally measured permeability. The original Kozeny model was identified as the most suitable model to predict the permeability of sand molds. Although the model predicts permeability well, the input parameters are laborious to measure. Hence, a methodology for replacing the pore diameter and tortuosity with simple process parameters is proposed. This modified version of the original Kozeny model helps predict permeability of foundry molds and cores at different regions resulting in better defect prediction and eventual scrap reduction.

Keywords: Permeability, Kozeny model, Density, Foundry core, Foundry mold, X-ray microtomography, Component casting, Cast iron

1. Introduction

Permeability in foundry molds and cores plays a vital role in producing sound and defect-free casting [1]. The permeability of sand molds determines the outgassing ability and the likelihood of detrimental defects in castings, such as blow holes, pinholes, and metal penetration. Sand molds and cores belonging to the consolidated porous media class are produced using methods such as hand ramming, jolt squeezing, core shooting, or additive manufacturing [2]. Although the goal is to produce molds and cores with optimum rigidity, strength, and permeability, regional variations in them are inevitable due to process conditions. This is especially true for molds and cores with complex geometries or those produced using core blowing or traditional molding methods [3]. The apparent density (will be referred to simply as density in

the rest of the paper) of the produced cores may bear local variations [4], and therefore, the cores may have different local permeabilities. Lannutti et al. studied the density variation in cores with methods such as X-ray computed tomography and acoustic stimulation, and discussed its effect on the quality of castings [5]. Korotchenko et al. in their work showed how casting simulation tools can predict the density variations in the cores produced with shooting/blowing process depending on the process parameters [6]. Winartomo et al. performed multiphase modelling of the core shooting process for an industrially used core with complex geometry. The authors obtained process parameters, such as mean grain size and the sand/solid fraction, to successfully model the possible density variations in the produced core [7]. Today, commercially available casting simulation tools predict properties, such as density and rigidity of large cores and molds, depending



on the geometry and the process conditions [8]. However, the available simulation tools still lack the ability to predict permeability in local regions. A predictive model that estimates permeability in local regions of cores/molds would be helpful in identifying potential defects in the cast component. Production parameters can be altered based on the results of the simulation resulting in reduced scrap and increased productivity.

Porosity, pore size distribution, and pore connectivity are factors that affect the permeability of a porous material [9]. Materials such as foundry samples can be treated as packed beds where the grain parameters and compactive effort act as the primary determinants of the porous structure. Grain parameters such as shape, size, and grain size distribution affect the permeability and porosity [10]. Compactive effort determines the packing of the grains and can increase or decrease the grain contact with other grains, thereby affecting the permeability [11]. Sand molds and cores are prepared using different binder systems. The binder in a sand mold creates 'bridges' that bind or hold the sand grains together [12]. The amount of binder used to prepare molds also influences the permeability of the molds and cores.

Only a handful of researchers in the field of casting have tried to predict the permeability of foundry molds and cores. Mitra et al. used the Kozeny-Carman equation to predict permeability and flow characteristics of sand molds prepared from additive manufacturing process [13]. However, less focus has been placed on the suitability and application criteria of the Kozeny-Carman equation for cores prepared using other production processes. Also the production parameters such as the grain diameter and porosity was not varied significantly. Ettemeyer et al. have used X-ray microtomography (μ CT) to study the strength, permeability, and thermal conductivity of foundry cores [14]. With respect to permeability, they used the obtained images from the tomography measurements to perform numerical simulations and computed the permeability from those images. The work does not consider modeling permeability based on a material's pore structure. There have been several attempts to predict permeability based on microstructural characteristics for other materials such as concrete [15,16]

The primary focus of the present work has been to compare the different models available to predict permeability by testing them on foundry core samples produced using different production parameters. The investigated foundry samples have been characterized using the non-destructive X-ray μ CT technique. X-ray μ CT is a powerful technique to investigate the interior of a material by reconstructing images [17]. The grain and pore parameters used in the models have been obtained using image analysis tools. The relationship between critical pore parameters and typical process parameters (such as grain size, porosity, and compactive effort) is identified, and a modified permeability model is proposed.

2. Methodology

2.1. Permeability Models

Researchers over the years have tried to predict the permeability of porous media using theoretical and empirical correlations. These correlations either target the attributes of the grains, such as grain size distribution, circularity, angularity, and roundness, or the pore structure parameters. Most of the earlier models developed treat the porous material as a bundle of capillaries, and either the Navier-Stokes equations or the Hagen-Poiseuille equation is solved for each capillary. Capillary models based on the Hagen-Poiseuille equation treating the problem with different assumptions are derived in the simple form, parallel capillary form, or series form. These attempts failed to predict permeability without introducing new additional parameters [18]. These models are developed from the basic assumption that the total velocity (also known as Darcian velocity) of the fluid at the outlet side is always less than the local pore velocity. This arises from the Dupuit-Forchheimer assumption for fluid flow.

$$v = \frac{q}{\phi} \quad (1)$$

where ϕ is the porosity, v is the total velocity (also known as the Darcian velocity), and q is the local pore velocity. The Darcian velocity is the average velocity of the fluid passing through a porous medium. The total volume flow, Q , through a capillary is given by the Hagen-Poiseuille equation,

$$Q = \frac{\pi D^4 dp}{128\mu dx} \quad (2)$$

where D is the diameter of the capillary, dp/dx is the pressure gradient across the length of the capillary, and μ is the viscosity of the fluid. Assuming there are several such capillaries and combining it with the Darcy law [19], the straight capillary (STC) case (Eq. 3) and serial capillary (SC) case (Eq. 4) models are obtained [18]. The STC model is given as follows:

$$k = \frac{\phi D^2}{32} \quad (3)$$

where k is the permeability. Since the simplest STC model does not represent the experimentally determined permeability values, researchers identified the need for a more complex model and derived the SC model by introducing an additional geometric parameter called tortuosity [20].

$$k = \frac{1}{96} \frac{\phi D^2}{T^2} \quad (4)$$

where T is the Tortuosity. Tortuosity can be given by the following relationship:

$$T = \frac{L_e}{L_0} \quad (5)$$

where L_e is the actual length of the pore, and L_0 is the shortest possible length. The more tortuous the paths for the fluid to traverse in the porous medium, the lesser the permeability of the medium is, and vice versa. Hence, porous media with a more complex structure is often found to be more tortuous in nature. Tortuosity increases with an increase in compaction. This has been observed in other materials, such as consolidated sandstones [21]. One of the most profound models to predict permeability is based on the Kozeny theory. In this model, the porous medium is assumed to be an assemblage of channels or cylindrical tubes of various cross-sections and a definite length [18]. The Kozeny equation was intended to predict permeability for different classes of materials spanning different research fields.

$$k = \frac{c\varphi^3}{(TS)^2} \quad (6)$$

where c is a material-specific constant, and S is the specific internal volume of the pores. The specific internal volume of the material is the ratio of the surface area of the imaginary channels to the volume of those channels.

Several researchers later modified the original Kozeny theory (OKT) model into different forms. One such modification is the Kozeny-Carman (KC) model which is widely used in many research fields. Several versions of the KC models exist in the literature. One such version is given by Eq. 7 [22].

$$k = \frac{D_g^2 \varphi^3}{180(1-\varphi)^2} \quad (7)$$

where D_g is the effective diameter of the grain. This version of the Kozeny-Carman model (Eq. 7) will be denoted as KC-1 for the rest of the paper. Another version (Eq. 8) of the Kozeny-Carman model (KC-2) that uses the specific surface area of the grains instead of the grain diameter is given as follows [23].

$$k = \frac{\varphi^3}{c(1-\varphi^2)S_g} \quad (8)$$

where S_g is the specific surface area of the grain, and c is a constant that depends on the shape of the pore. This constant, c , varies according to the type of material that is being studied.

Another method to model the permeability of porous material is to use the hydraulic radius model (HR). The hydraulic diameter for non-circular channels is given by Eq. 9,

$$D_h = \frac{4A}{P} \quad (9)$$

where D_h is the hydraulic diameter, P is the perimeter of the channel, and A is the surface area of the channel. With the D_h , no losses in the pore channel are expected since it is calculated without assuming any shapes for the pores. The HR model for permeability prediction based on Slichter's [24] work is provided in Eq. 10.

$$k = \frac{nD_h^2}{96(1-\varphi)} \quad (10)$$

where n is the area of the passage for fluid or simply the pore area. Slichter, in his work, estimated n based on theoretical

considerations and found it to fall in the range of 0.0931 – 0.2145. The value for n was estimated theoretically based on sphere packing theory for porosities in the range of 26% (the tightest) to 48% (loosest packing) [25].

2.2. Material Characterization

The experimental methodology includes, the preparation of samples, experimental permeability measurement and investigation of the measured samples. Foundry samples were prepared in two different steps. In the first step, samples were prepared with varying average grain size values. This was achieved by altering the amount (percentage) of 0.125 mm grains in the base sand. The base sand had an average grain size of 0.31 mm and had 10% of 0.125 mm grains. The resulting samples had average grain sizes of 0.33, 0.28, and 0.24 mm (samples A, B, and C). The samples had 0%, 20% and 40% of 0.125 mm grains, respectively. The average grain size values presented were estimated based on the calculation using multipliers from the sieve analysis results. The second set of samples had varying densities. The density of the samples was varied by altering the amount of sand added to the rammer tube setup. The resulting samples had density values of 1.36 and 1.52 g/cm³, respectively (samples D and E). Other parameters were kept constant for all five samples. The properties of the prepared samples are presented in Table 1. The prepared samples (with 50 × 50 mm dimension) were then subjected to permeability measurements using a custom-made measurement setup [26,27]. The resulting permeability values are also shown in Table 1. The samples were prepared using 2% of furan resin. A sulphonic acid based catalyst was used for the hardening process (40% of the weight of the binder was added as the catalyst).

Table 1. The properties of the investigated samples prepared with 2% furan binder

Sample	Density (g/cm ³)	Average grain size (mm)	Experiemental permeability (m ²)
A	1.45	0.33	2.05×10 ⁻¹²
B	1.45	0.28	1.04×10 ⁻¹²
C	1.47	0.24	0.96×10 ⁻¹²
D	1.39	0.31	5.26×10 ⁻¹²
E	1.51	0.31	1.43×10 ⁻¹²

Two characterization techniques were employed to study the pore characteristics and the porous microstructure of the material. Traditional mercury intrusion porosimetry was utilized to study the essential pore characteristics such as the pore size distribution, the open porosity, etc. The detailed results of mercury porosimetry (MP) measurements have been published in previous work [26]. Aggregate parameters like circularity, grain size distribution, and other pore structure-related factors were studied by X-ray μ CT, and the obtained images were studied to estimate these parameters. This work primarily focuses on measuring geometric characteristics such as tortuosity, specific internal volume, and hydraulic diameter using image analysis. A 14 × 14 mm section of the sample was cut

from each of the five samples, and X-ray μ CT evaluation was performed. A 14×14 section would result in a sample volume of 2700 mm^3 (which, according to the literature, is a good representative elementary volume value of the sample [28]). X-ray μ CT evaluation was performed using microfocus CT equipment (GE v|tome|x m) with a reconstructed voxel size of $\sim 3 \mu\text{m}^3$. The obtained image slices (Fig 1a) were analyzed using Fiji, an open-source image processing and analysis tool [29].

The obtained images provided an opportunity to determine the size and shape of the grains accurately. Circularity was measured based on the standard definition used in particulology [30]. However, since tomography was performed on bonded samples, the binder bridges were also captured in the obtained images (Fig 1b). In order to tackle this issue, watershed segmentation was performed to separate the grains (Fig 1c), and the individual particles (Fig 1d) were then analyzed to determine their shape and size [31]. The segmented images were analyzed using the particle analysis plugin in Fiji. Grain parameters such as circularity,

roundness, grain size, grain area, pore area, and perimeter of the grains were obtained. Using the pore area and the perimeter obtained from the results, the hydraulic diameter of the samples was computed.

The porosity of the sample was measured using the fraction tool available in the BoneJ plugin [32]. Porosity values obtained from image analysis are compared with those obtained from mercury porosimetry to find the differences observed between the two characterization techniques. For the measurement of pore size distribution, the local thickness tool of the BoneJ plugin was employed [33]. For the pore size measurement, slices were not subjected to watershed segmentation. A histogram of the pore diameter data was obtained from the measurement results (Fig 1e). The pore diameter data is used to compute the geometric parameters like the surface area, volume, and the specific internal volume of the channel. In order to measure the tortuosity, the 2D images were reconstructed using the 3D viewer plugin of Fiji [34].

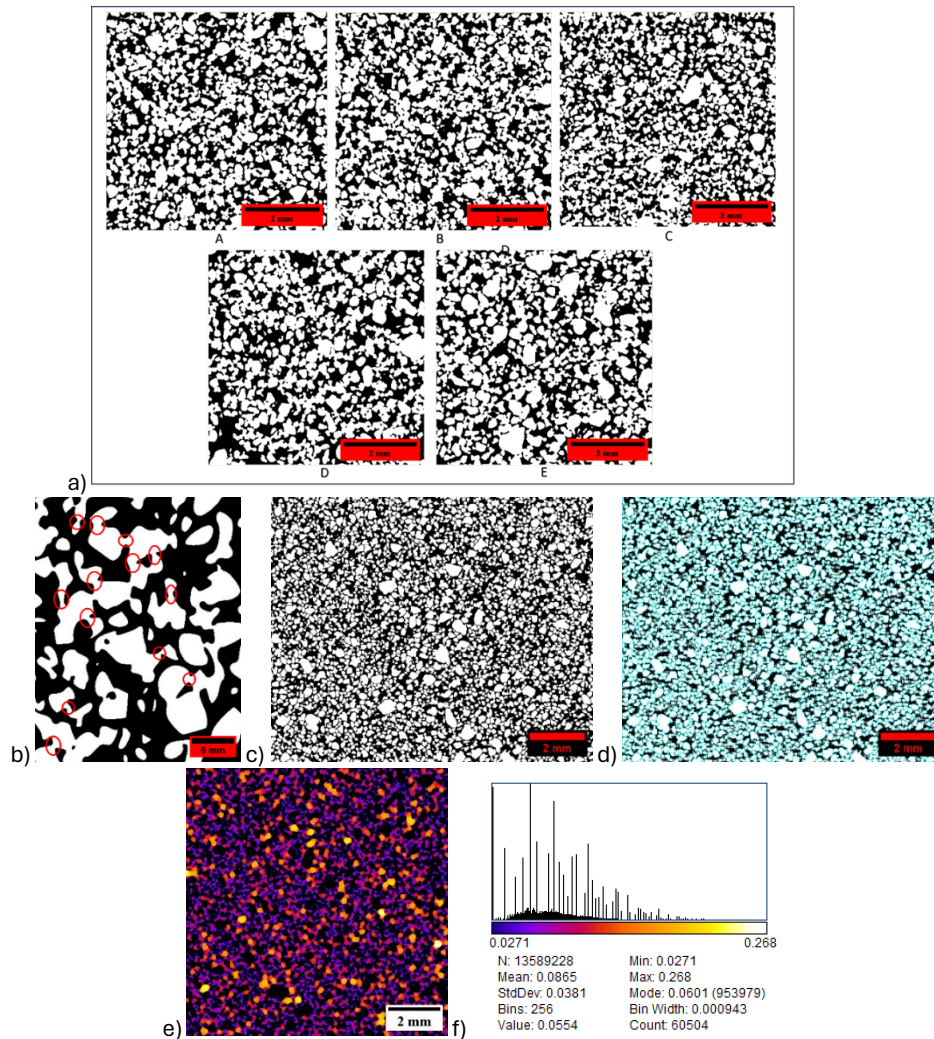


Fig. 1. The experimental methodology for the measurement of grain/aggregate and the pore structure parameters. (a) Obtained slices of the different samples. (b) Binder bridges identified for the samples. (c) Slice after removal of binder bridges. (d) Grain parameters (overlaid on Fig 1c) studied using the particle analysis tool. (e) The pore size distribution obtained using the local thickness tool

2.3. Derivation of Modeling Parameters

Grain Parameters

Table 2.
Circularity and average grain diameter computed with image analysis (IA) and sieve analysis (SA)

Sample	Grain diameter (μm)			Circularity
	Median D_{mg}	Mean, (IA)	Mean, (SA)	
A	233	247	330	0.79
B	220	238	280	0.78
C	208	228	240	0.78
D	236	251	310	0.79
E	225	240	310	0.78

Although grain size distribution can roughly be estimated by traditional methods such as sieve analysis, it must be remembered that it only provides a rough estimate because of the nature of the measurement. The technique uses sieves of different size ranges, and grains that get segregated into a particular sieve may be of different sizes within the limit of the next sieve. This study estimated grain size distribution and actual grain diameter from image analysis tools, and the results are presented in Table 2. From the grain size distribution, several percentile values were tested to find the effective grain diameter to be used in the KC models. The percentile values providing the most significant difference between the samples fell in the 40th to 60th percentile, out of which the median grain diameter, D_{mg} , was identified as the effective diameter that genuinely differentiates the samples. The average grain diameter measured from image analysis shows that the mean

value is much smaller than the traditional average grain size calculation done using sieve analysis and multipliers. The traditional method can also inflate the difference in the grain size distribution between batches. A decrease of roughly 10 μm was noticed between A, B, and C. Sample D and E had no change in grain size distribution. However, the results show that the mean for sample B is much lower than for sample A. Traditional sieve analysis did not capture this difference. The circularity did not vary much between the samples, which shows that the shape of the grains of the foundry sand is relatively uniform throughout, even for varying size fractions. The specific surface area, S_G , provided in the KC-2 is the surface-to-volume ratio of the particles. In this case, it was calculated by the simple formula $6/D_g$, where D_g is the effective diameter of the grain (identified to be the median grain diameter, D_{mg}).

Table 3.
The experimentally obtained pore structure parameters using both image analysis (IA) and mercury porosimetry (MP)

Sample	ϕ (IA)	ϕ (MP)	$D_h, \mu\text{m}$		T	$h, \mu\text{m}$
			Mean	(IA) (MP)		
A	0.45	0.43	145	106 71	1.025	128.0
B	0.45	0.43	143	100 69	1.238	125.3
C	0.44	0.45	126	87 65	1.245	118.0
D	0.48	0.48	164	129 101	1.027	140.8
E	0.43	0.43	127	99 69	1.238	128.6

Pore structure parameters

The porosity, pore diameter and tortuosity of the samples was measured from the obtained images. The results (including results from mercury porosimetry) are presented in Table 3.

The results show that with image analysis, the difference in porosity between the samples is measured as accurately as the mercury porosimetry technique. However, the results obtained through porosimetry always show a slightly reduced value. The authors hypothesize that this difference is due to the nature of the measurement itself, wherein only open pores are measured with mercury porosimetry. At the same time, the image analysis technique captures the blind pores, too and hence, the values are slightly higher. The difference between these two methods could roughly be deemed as the fraction of blind pores in foundry samples.

The pore diameter is one of the most important parameters for modeling permeability. The median pore diameter, D_{mp} , was

identified as the effective pore diameter to be used in the prediction models. The average value is usually misleading because of the skewed nature of the distribution curves. Pores in a porous material are considered to be channels/cylinders of a particular cross-section, and the area and volume of the cylindrical channels determine the permeability.

The median pore diameter measured from the images and the values obtained from porosimetry have also been reported for comparison. It is worth noting that the median pore diameter obtained from mercury porosimetry was lower than in the image analysis technique. This is not surprising since the pore size distributions obtained using porosimetry could be significantly different from the pore size distribution data obtained from image analysis for certain materials due to the differences in the nature of measurement [35]. The median pore diameter decreases as the average grain diameter decreases for samples with similar densities (A, B, and C). A significant reduction in median pore diameter was

noted for samples with increasing densities (D and E) A sharp decrease in the experimentally determined permeability was also seen for these samples. The tortuosity results show that with decreasing average grain diameter, there is an increase in tortuosity (A, B, and C). Also, with increasing density, the samples become more tortuous (D and E). The results of the pore height, h , (the height of the cylindrical capillary) are also presented in Table 3. The pore height was seen to increase with increasing grain diameter.

Specific internal volume

The specific internal volume (or the surface area of the pores) that the Kozeny equation includes was computed using the median pore diameter obtained from image analysis and MP. These results were later compared to identify which of these methods provide the best accuracy. Table 4 provides the values of the specific internal volume calculated from image analysis and mercury porosimetry. Since the specific internal volume calculation also needs the pore's height, it adds an additional parameter and complexity to the estimation. Hence, the possibility of simply assuming the pores to be comprised of cylinders with the same height as the diameter was also considered (Table 4).

Table 4.

The results of the calculated specific internal volume for different pore shapes using image analysis (IA) and mercury porosimetry (MP).

Sample	Specific internal volume (m^2/m^3)		
	D_{mp} (IA)	D_{mp} (MP)	$D_{mp} = h$ (D_{mp} from MP)
A	37915	56077	84116
B	40201	57695	86542
C	45977	61228	91841
D	31008	39604	59405
E	40404	57971	86956

3. Results and discussion

3.1. Modeling results

Capillary Models

Median pore diameter and porosity measured using both image analysis and mercury porosimetry were tested in the permeability models. Permeability predicted using the capillary models showed several orders of magnitude deviation from the experimental results, which shows that the capillary models are unsuitable for predicting the permeability of complex porous systems such as molds and cores.

Hydraulic Radius model

The pore area, n , was estimated based on the obtained images. The estimated pore area values are presented in Table 5.

Table 5.

The pore area values were measured using image analysis

Sample	Pore area (m^2)
A	2.24×10^{-2}
B	2.11×10^{-2}
C	1.71×10^{-2}
D	2.74×10^{-2}
E	1.70×10^{-2}

Although the predicted results were in the order of magnitude of the measured values, the results were not accurate in predicting the permeability variation between the samples. From the results, the D_h is observed to be significantly greater than the median pore diameter obtained from image analysis and mercury porosimetry. This was expected since hydraulic diameter measurement includes the pore area and perimeter instead of assuming a shape for pore capillaries. Assuming a certain shape (such as a cylinder) results in neglected regions, resulting in reduced values.

Kozeny-Carman models

Permeability was estimated based on median grain diameter, D_{mg} , which was identified as the effective grain diameter value used in the KC models. Essentially, both versions of the KC model are the same since both use the diameter (directly in KC-1 and indirectly in KC-2). The difference between the two models lies in the fitting constant. KC-1 has a fixed constant of 180, while with KC-2, a modified value for the constant c is possible. The constant c is empirically estimated to be 5 for perfectly spherical particles. Using $c = 5$ in KC-2 would result in the same values for permeability as in KC-1. For the studied samples, c was experimentally estimated to be 56, based on the least squares method.

The KC models primarily assume a particular type of packing because of free-flowing grains, however, in the case of foundry molds and cores, additional aspects are involved. The use of resin/catalyst significantly reduces the flowability of sand and, therefore, the packing. Compaction/consolidation further alters the packing of the grains. These additional factors make the prediction of permeability based only on the grain size distribution or the effective grain diameter of foundry sands hard and invalid. Therefore, KC-1 and KC-2, which are widely used for predicting permeabilities can be deemed as ineffective models for consolidated material such as foundry molds and cores.

The Kozeny-Carman model might work better with additively manufactured sand molds/cores. Since the additive manufacturing process does not involve compactive effort and the method can produce cores and molds from a single grain size, it can predict the permeability in those cases with a certain degree of accuracy. However, the addition of binder and, therefore, the changes to the porosity and pore structure are not considered in the KC models. Hence, slight modifications must be done even in these cases to improve the accuracy. Regarding molds and cores produced using core blowing and traditional molding processes, KC models are not suitable for permeability prediction.

Original Kozeny model

The OKT model predicts permeability using tortuosity, pore diameter, and porosity. Including these parameters makes the

model robust since these parameters are sensitive to the effects of compaction. Median pore diameter, D_{mp} , from image analysis and mercury porosimetry were tested. The results show that calculating specific internal volume (S) using the mercury porosimetry median pore diameter measurements provided more accurate results when compared with the S calculated using the median pore diameter obtained from image analysis. Since all the remaining parameters were known, the constant c was estimated to be 0.076 based on the least squares method.

Although the model uses the concept of specific internal volume, which assumes cylindrical pores (with different lengths), the model predicted permeability with similar accuracy if the pores were assumed to have the same diameter and height. This

assumption removes the need to measure the height of the cylindrical pores. However, with this assumption, the constant became 0.17. It can be concluded that the OKT model could be used for predicting the permeability of molds and cores if median pore diameter, tortuosity, and porosity are known.

The obtained parameters were incorporated into the available permeability models for comparison to find the most suitable model in terms of predictive accuracy. The STC and KC-1 models use only two parameters to predict permeability. KC-2, OKT and the HR model use three parameters to predict permeability. The predicted permeability results using the different models and the experimental values are presented in Table 6.

Table 6.

Permeability values were obtained from the tested models in comparison with experimental measurement. (STC - straight capillary model, SC - series capillary, KC-1 - Kozeny Carman model -1, KC-2 - Kozeny Carman model 2, OKT - original Kozeny theory model, HR - hydraulic radius model).

Sample	Permeability (m^2)						Experimental
	STC	SC	KC-1	KC-2	OKT	HR	
A	1.55×10^{-10}	4.93×10^{-11}	8.96×10^{-12}	2.10×10^{-12}	2.02×10^{-12}	8.87×10^{-12}	2.05×10^{-12}
B	1.38×10^{-10}	3.01×10^{-11}	8.82×10^{-12}	1.88×10^{-12}	1.32×10^{-12}	8.15×10^{-12}	1.04×10^{-12}
C	1.04×10^{-10}	2.24×10^{-11}	8.07×10^{-12}	1.59×10^{-12}	1.10×10^{-12}	5.06×10^{-12}	0.96×10^{-12}
D	2.51×10^{-10}	7.92×10^{-11}	0.12×10^{-12}	2.82×10^{-12}	5.07×10^{-12}	0.15×10^{-12}	5.26×10^{-12}
E	1.31×10^{-10}	2.86×10^{-11}	7.11×10^{-12}	1.70×10^{-12}	1.15×10^{-12}	5.01×10^{-12}	1.43×10^{-12}

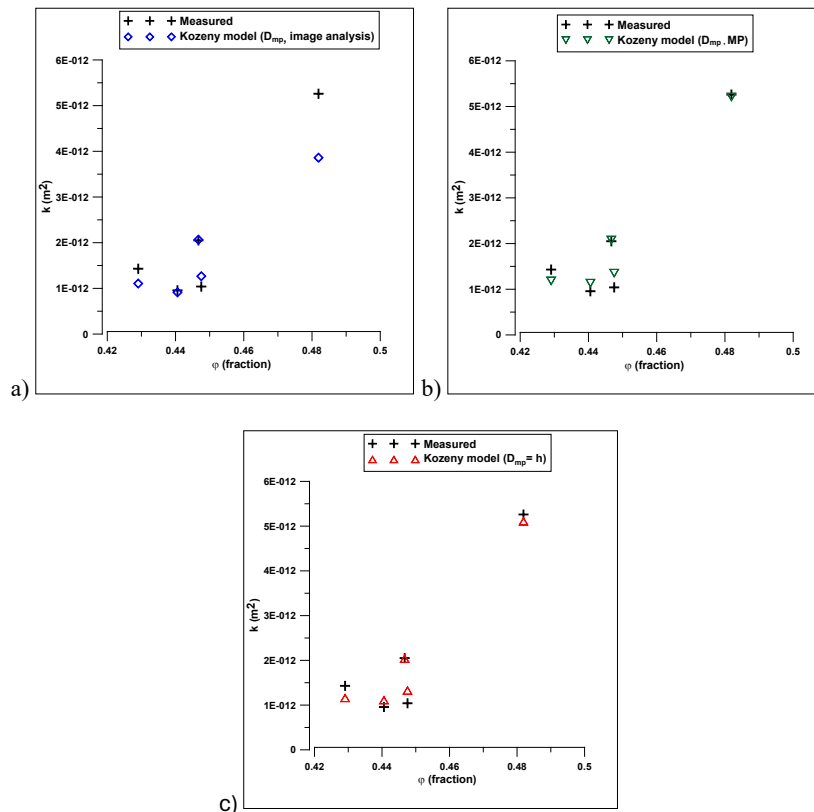


Fig. 2. The predicted and experimental permeability values plotted against the porosity of the investigated samples. (a) Median pore diameter from image analysis, (b) Median pore diameter by mercury porosimetry (c) Median pore diameter by mercury porosimetry (neglecting the pore height)

Fig 2a shows the results of predicted permeability with specific internal volumes calculated using the median pore diameter obtained from image analysis. Fig 2b shows the results of the predicted permeability, where the specific internal volume was calculated using D_{mp} values obtained from mercury porosimetry. Fig 2c shows the results of predicted values when the specific internal volume was calculated using the D_{mp} obtained from

mercury porosimetry, but neglecting the pore height (i.e., assuming pore diameter and pore height to be equal).

Summary of the modeling results

Several models (theoretical and empirical) were tested for foundry samples. The results show that the OKT model, which includes the effect of compaction, is the most accurate (refer Fig 3).

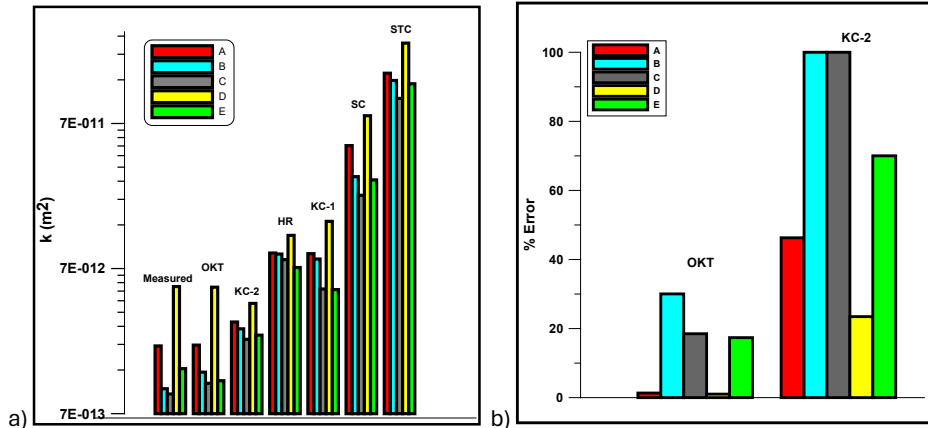


Fig 3. Modeling results plotted together with the experimental results¹ (a). The percentage error shown for OKT model and KC-2 model¹ (b)

¹STC - straight capillary model , SC – series capillary, KC-1 – Kozeny Carman model -1, KC-2 – Kozeny Carman model 2, OKT – original Kozeny theory model, HR – hydraulic radius model.

Table 7 provides a summary of the permeability models evaluation. The OKT model was found to be the most suitable model for estimating the permeability of foundry cores and molds based on the accuracy of the obtained results. Theoretically, the model is

robust since it also incorporates the effect of consolidation/compaction. The model enables prediction of permeability for foundry samples produced from different processes.

Table 7. Summary of the permeability models evaluation

	Straight Capillary	Series Capillary	Kozeny-Carman 1	Kozeny-Carman 2
Model	$k = \frac{\varphi D^2}{32}$	$k = \frac{1}{96} \frac{\varphi D^2}{T^2}$	$k = \frac{D_g^2 \varphi^3}{180(1 - \varphi)^2}$	$k = \frac{\varphi^3}{c(1 - \varphi^2)S_g}$
Type	Pore space based	Pore space based	Particle based	Particle based
Parameter	Porosity, φ Pore diameter, D	Porosity, φ Pore diameter, D Tortuosity, T	Porosity, φ Effective grain Diameter, D_g	Porosity, φ Specific surface area of grain, S_g
Specific fitting constant?	No	No	No	Yes (Estimated, $c= 56$)
Accuracy	Poor	Poor	Poor	Poor
Observation	Simplicity of the model and additional complications in the production of molds and cores make it unsuitable.	Unsuitable because of lack of material specific constant resulting in deviation of several orders of magnitude from experimental results.	Unsuitable because of the nature of packing assumed in the model and also since molding materials involves compaction.	Unsuitable because of the nature of packing assumed in the model and also since molding materials involves compaction.

Table 7. (Continued)

	Original Kozeny	Hydraulic radius
Model	$k = \frac{c\varphi^3}{(TS)^2}$	$k = \frac{nD_h^2}{96(1-\varphi)}$
Type	Pore Space based	Pore Space based
Parameter	Porosity, φ Tortuosity, T Specific internal Volume, S	Porosity, φ Pore area, n Hydraulic diameter, D_h
Specific fitting constant?	Yes (Estimated $c=0.07$ and when $D_{mp} = h$, $c = 0.17$)	No
Accuracy	Good	Poor
Observation	Most suitable model and recommended for predicting the permeability of all types of foundry molds and cores	Unsuitable because of the usage of hydraulic diameter which overestimates the fluid passage area.

3.2. Different length scales to characterize permeability

All the permeability models include a length scale, and this length scale, in combination with porosity, is used for characterizing permeability. The results show that the median pore diameter is better in predicting permeability in comparison to the others. For example, hydraulic diameter does not characterize the permeability well. This could be because of the non-uniformity of the porous channels, the hydraulic diameter, which includes the perimeter and area of a pore, results in an overestimation of the characteristic length scale. On the other hand, the median pore diameter, which is estimated by assuming a certain shape for the pores, results in a lower value that characterizes permeability better.

3.3. Derivation of compaction factor

The evaluated models show that in order to predict permeability of compacted granular systems like foundry molds and cores accurately, parameters such as pore diameter and tortuosity are necessary. However, measuring parameters such as tortuosity and pore diameter is laborious. The ability to predict the pore diameter and tortuosity using more straightforward and simple-to-measure parameters would become very convenient from a practical viewpoint. For materials such as sandstones, a modification was done based on the relevant properties of those materials, such as formation factor, cementation factor, porosity, etc. [36].

The number of grains in a sample depends on the degree of compaction and the size of the grains. The number of grains increases with smaller grain size and vice versa. Also, the number of grains increases with increasing compactive effort. The number

of grains can be estimated from the measurements using the relationship between the pore volume, solid volume, and porosity.

$$\varphi = \frac{V_p}{V_{tot}} \quad (11)$$

where φ is the porosity, V_p is the pore volume, and V_{tot} is the total volume (i.e., pore volume + solid volume). Assuming the grains to be perfect spherical particles, the total volume would be given as,

$$V_s = N \cdot \frac{4}{3}\pi R^3 \quad (12)$$

where V_s is the solid volume, N is the number of grains, and R is the radius of the spherical grain. Assuming a certain total volume, V_{tot} , the number of grains can be estimated by Eq. 13

$$N = \frac{(1-\varphi) \cdot V_{tot}}{\frac{4}{3}\pi R^3} \quad (13)$$

Theoretically, the minimum achievable porosity with spherical grains in a system is 0.26 ([25],[37]). Assuming this state of the system to be the most compacted, the number of grains for this ideal case at a particular grain diameter can be estimated. Based on this approach, a compaction factor, f_c of 1, is assigned to the ideal case where there is no difference between the maximum possible number of grains and actual number of grains. For the studied samples, the relative difference between this maximum possible number of grains and the actual number of grains (Fig 4) was estimated, assuming the V_{tot} to be 10 mm³. Based on this difference, the compaction factor was determined as the sum of 1 and the fraction of decrease from the ideal case. For example, in sample A, this fraction would be 0.2524. Therefore, the compaction factor is estimated as 1.2524. The more a sample deviates from the ideal value 1, the less compact the sample is. The results of the

computed compaction factor, f_c using the number of grains is presented in Table 8.

Table 8.
The calculated compaction factor for the measured samples.

Sample	Actual number of grains	Maximum possible number of grains	f_c
A	835	1117	1.2524
B	991	1327	1.2534
C	1187	1571	1.2439
D	753	1075	1.2999
E	957	1241	1.2284

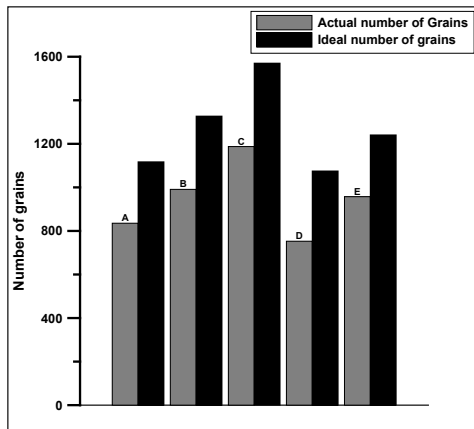


Fig 4. The actual number of grains in each sample along with the maximum possible number of grains corresponding to the ideal case

Only if the compactive effort is similar, samples with different median grain diameters can have the same porosity. On the other hand, it is possible to have the same median grain diameter and different porosities depending on the compactive effort applied. In the present work, the grain diameter varied for the different samples. For samples A, B, and C, the difference in compaction factor is meager, although the median grain diameters were different, which indicates the compactive effort was roughly the same. For samples D and E, the compactive effort differed relatively more, even though there was a difference in the grain diameters. In a scenario where the grain diameters are similar, and there is a difference in the compactive effort (like in cores produced through the blowing process), the compaction factor, median grain diameter, and porosity would determine the pore diameter and tortuosity of the material. Based on this method, the compaction factor for any material can be estimated using the grain diameter and the porosity.

3.4. Modification of the OKT model

The OKT model when assuming the median pore diameter and height of the cylindrical pore are equal (neglecting the need to measure the pore height) can be rewritten as Eq. 14, by

incorporating the term $(6/D_{mp})^2$ for specific internal volume (or specific surface area) of the pore capillary into Eq. 6,

$$k = \frac{c\varphi^3}{36} \cdot \frac{D_{mp}^2}{T^2} \quad (14)$$

Physically, the term D_{mp}/T should be a function of the median grain diameter, porosity, and compaction factor, which directly correlates with the pore diameter.

$$\frac{D_{mp}}{T} = f(D_{mg}, \varphi, f_c) \quad (15)$$

Theoretically, porosity is independent of the pore diameter. Hence for the same porosity, the pore diameter could be different. Larger compaction factor (low compactive effort) scales up the porosity ($\varphi \cdot f_c$). It creates a larger difference in the scaled-up porosity between samples and introduces a functional relationship with the pore diameter, $D_{mp} = f_1(\varphi \cdot f_c)$. Similarly, pore diameter increases with grain diameter. Therefore, $D_{mp} = f_2(D_{mg} \cdot \varphi \cdot f_c)$, where f is a monotonically increasing function with the graph passing through the origin. Also, it is known from the literature that tortuosity increases for higher compaction (i.e., lower f_c) and decreasing porosity. It means that $1/T = f_3(\varphi \cdot f_c)$. Therefore, it is reasonable to represent D_{mp}/T as Eq. 16.

$$\frac{D_{mp}}{T} = f(k_0) \quad (16)$$

where k_0 is given as,

$$k_0 = D_{mg} \cdot \varphi \cdot f_c \quad (17)$$

The k_0 value was calculated for the samples, and the results are presented in Table 9. Even though a strict theoretical relationship between the parameters in Eq. 15 and 16 is hard to establish, it is known that some correlations can be described by power law. For instance, the relationship between porosity, φ , and tortuosity, T , is given by the Bruggeman model [38]. Therefore, the correlation function between experimentally determined D_{mp}/T and k_0 was assumed to obey power law with two fitting parameters, as shown in Fig 5.

Table 9.
The calculated k_0 values with corresponding D_{mp}/T for the studied samples

Sample	D_{mp}/T (m)	k_0 (m)
A	6.93×10^{-5}	1.30×10^{-4}
B	5.56×10^{-5}	1.23×10^{-4}
C	5.22×10^{-5}	1.14×10^{-4}
D	9.83×10^{-5}	1.48×10^{-4}
E	5.58×10^{-5}	1.19×10^{-4}

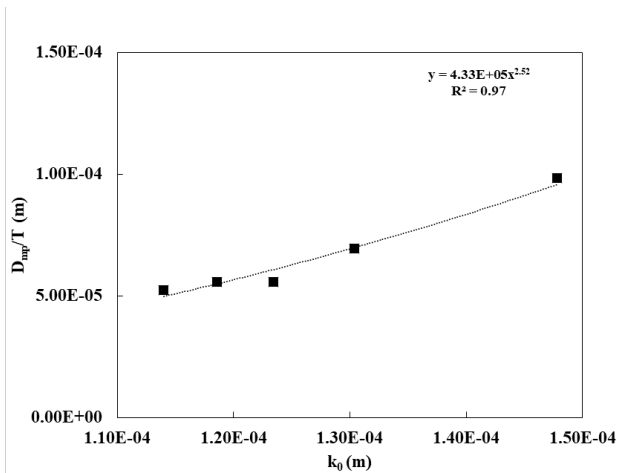


Fig 5. The graph shows the pore diameter divided by tortuosity plotted against the term k_0 .

The empirical relationship between D_{mp}/T and k_0 is given by the power law as follows:

$$\frac{D_{mp}}{T} = 4.33 \cdot 10^5 k_0^{2.52} \quad (18)$$

The modified version of the OKT model can now be written as Eq. 19.

$$k = \frac{c\varphi^3(4.33 \cdot 10^5 k_0^{2.52})^2}{36} \quad (19)$$

where $c = 0.17$ for the studied foundry samples. The permeability values obtained from the modified version of the Kozney model are presented in Table 10.

Table 10. The results of the estimated and experimental permeability

Sample	Permeability (m^2)	
	Modified OKT model	Experimental
A	2.04×10^{-12}	2.05×10^{-12}
B	1.56×10^{-12}	1.04×10^{-12}
C	0.99×10^{-12}	0.96×10^{-12}
D	4.83×10^{-12}	5.26×10^{-12}
E	1.12×10^{-12}	1.43×10^{-12}

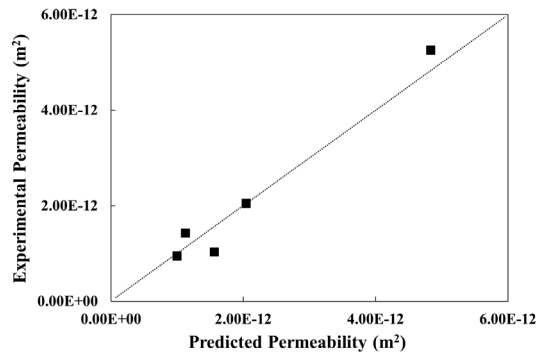


Fig 6. The experimentally obtained permeability plotted against the predicted permeability computed using the modified version of the original Kozeny model (Equation.19).

The results show that the new model that uses typical, easy-to-obtain parameters can predict permeability accurately. Fig 6 shows the experimentally obtained values plotted against the predicted values.

The modified model enables permeability prediction for different regions of cores and molds with complex geometries using the median grain diameter, the porosity (or solid fraction), and the compaction factor. The median grain diameter can be measured accurately using tools such as laser diffraction or dynamic image analysis. The regional porosity can be estimated with commercially available core shooting simulation tools. The proposed model is applicable for porous materials with a porosity in the range of 0.26-0.60. This range encompasses the maximum and minimum porosities that foundry mold and core samples are prepared with.

4. Conclusions

Foundry samples were investigated using X-ray μ CT to estimate all necessary parameters to model permeability through cores and molds. A comparison of the median pore diameter obtained from mercury porosimetry was also done to find out the most effective method. These parameters were incorporated into several models available in the literature to evaluate and identify the most suitable one to predict permeability. A modification of the most suitable model is also proposed based on the obtained parameters. With the modified version, the measurement of laborious parameters such as pore diameter and tortuosity can be avoided, and permeability at local regions can be predicted for all foundry sand molds and cores. The following conclusions can be made from the current work.

- Traditional sieve analysis estimation of the average grain diameter results in exaggerated values.
- The median grain diameter value, D_{mg} , is the most representative in differentiating samples with different grain size distributions typically found in foundry sands.
- To estimate permeability, the median pore diameter is the most accurate of all the different length scales. The hydraulic diameter seems to overestimate permeability significantly.

- The Kozeny-Carman model is not effective in predicting the permeability of foundry samples prepared from molding and blowing processes. Researchers need to be careful when using the KC, even for core/mold-making processes such as binder jetting, which do not include any compaction because the binder bridges affect the specific surface area and pore structure of the material.
- The most suitable model for predicting the permeability of all types of sand cores and molds is the original Kozeny theory-based model.
- A new parameter, compaction factor, that quantifies the effect of compaction was introduced.
- A new term, k_0 , was proposed to replace the median pore diameter and tortuosity from the original Kozeny theory model, resulting in the modification of the model.
- When combined with the simulation of core shooting, the modified model helps predict permeability in local regions, enabling better defect prediction during the casting of complex components.
- The modified model can be used to predict the permeability of all types of foundry sand molds and cores.

Acknowledgement

This work was made possible through the IFT: JÖNKÖPING project (Grant Number 20210082), co-financed by the Swedish Knowledge Foundation, Jönköping University, Scania CV AB, Volvo Group Trucks Technology AB, SinterCast AB, Bruzaholms Bruk AB and SKF Mekan AB.

Disclosure

The authors declare no conflict of interest

List of symbols and Abbreviations

ϕ	Porosity
μ	Viscosity of the fluid
v	Total velocity of the fluid passing through a porous body
q	Velocity of the fluid in the pore
Q	Total volume flow
dp/dx	Pressure gradient across the length of the capillary
T	Tortuosity
L_e	Actual branch length
L_0	Shortest possible length across a branch
c	Material specific constant used in some permeability models
S	Specific internal volume
k	Permeability
P	Perimeter of the pore
A	Surface area of the pore
n	Area of the pore
h	Height of the cylindrical pore
R	Radius of the spherical grains
D	Diameter of the capillary
D_h	Hydraulic diameter

D_g	Effective grain diameter
D_{mg}	Median grain diameter
D_{mp}	Median pore diameter
V_p	Pore volume
V_s	Solid volume
V_{tot}	Total volume
N	Number of grains
R	Effective radius of the grain
f_c	Compaction factor
k_0	The product of D_{mg} , f_c and ϕ

References

- [1] Jorstad, J., Krusiak, M.B., Serra, J.O., La Fay, V. (2018). Aggregates and binders for expendable molds. Casting. 528-548. <https://doi.org/10.31399/asm.hb.v15.a0005242>.
- [2] Campbell, J., Svidr6, J.T. & Svidr6, J. (2017). Molding and Casting Processes. In Doru M. Stefanescu (Eds.), Cast Iron Science and Technology (pp. 189-206). ASM International. <https://doi.org/10.31399/asm.hb.v01a.a0006297>.
- [3] Ramakrishnan, R., Griebel, B., Volk, W., Günther, D. & Günther, J. (2014). 3D printing of inorganic sand moulds for casting applications. Advanced Materials Research. 1018, 441-449. <https://doi.org/10.4028/www.scientific.net/AMR.1018.441>.
- [4] Dańko, R. & Jamrozowicz, Ł. (2017). Density distribution and resin migration investigations in samples of sand core made by blowing method. Journal of Casting & Materials Engineering. 1(3), 70-73. <https://doi.org/10.7494/jcme.2017.1.3.70>.
- [5] Lannutti, J.J., Mobley, C.E. (2003). Improvements in Sand Mold/Core Technology: Effects on Casting Finish. Final Technical Report, The Ohio State University, Columbus, OH.
- [6] Korotchenko, A.Y., Khilkov, D.E., Khilkova, A.A. & Tverskoy, M.V. (2020). Improving the quality of production of sand core on core shooting machines. Materials Science Forum. 989, 589-594. <https://doi.org/10.4028/www.scientific.net/MSF.989.589>.
- [7] Winartomo, B., Vroomen, U., Bührig-Polaczek, A. & Pelzer, M. (2005). Multiphase modelling of core shooting process. International Journal of Cast Materials Research. 18(1), 13-20. <https://doi.org/10.1179/136404605225022811>.
- [8] Thorborg, J., Wendling, J., Klinkhammer, J., Heitzer, M. (2023). Modelling hot distortion of inorganic bonded sand cores and application on complex 3D printed automotive cores, IOP Conference Series: Materials Science and Engineering. 1281(1), 012069. <https://doi.org/10.1088/1757-899x/1281/1/012069>.
- [9] Muskat, M. (1937). The flow of fluids through porous media, Journal of Applied Physics. 8(4), 274-282. <https://doi.org/10.1063/1.1710292>.
- [10] Campbell, J. (2011). Molds and cores. Complete Casting Handbook. 1, 155-186. <https://doi.org/10.1016/b978-1-85617-809-9.10004-0>.
- [11] Marks, B., Sandnes, B., Dumazer, G., Eriksen, J.A. Måløy, K.J. (2015). Compaction of granular material inside confined geometries, Frontiers in Physics. 3, 1-9. <https://doi.org/10.3389/fphy.2015.00041>.

- [12] Bargaoui, B., Azzouz, F., Thibault, D. & Cailletaud, G. (2017). Thermomechanical behavior of resin bonded foundry sand cores during casting. *Journal of Materials Processing Technology*. 246, 30-41. <https://doi.org/10.1016/j.jmatprotec.2017.03.002>.
- [13] Mitra, S., EL Mansori, M., Rodríguez de Castro, A. & Costin, M. (2020). Study of the evolution of transport properties induced by additive processing sand mold using X-ray computed tomography. *Journal of Materials Processing Technology*. 277 116495. <https://doi.org/10.1016/j.jmatprotec.2019.116495>.
- [14] Etmeyer, F., Lechner, P., Hofmann, T., Andrä, H., Schneider, M., Grund, D., Volk, W. & Günther, D. (2020). Digital sand core physics: Predicting physical properties of sand cores by simulations on digital microstructures. *International Journal of Solids Structures*. 188-189, 155-168. <https://doi.org/10.1016/j.ijsolstr.2019.09.014>.
- [15] Neithalath, N., Sumanasooriya, M.S. & Deo, O. (2010). Characterizing pore volume, sizes, and connectivity in pervious concretes for permeability prediction. *Materials Characterization* 61(8), 802-813. <https://doi.org/10.1016/j.matchar.2010.05.004>.
- [16] Das, S., Stone, D., Convey, D. & Neithalath, N. (2014). Pore and micro-structural characterization of a novel structural binder based on iron carbonation, *Materials Characterization*. 98, 168-179. <https://doi.org/10.1016/j.matchar.2014.10.025>.
- [17] Landis, E.N. & Keane, D.T. (2010). X-ray microtomography. *Materials Characterization*. 61(12), 1305-1316. <https://doi.org/10.1016/j.matchar.2010.09.012>.
- [18] Scheidegger, A.E.. (1957). *The physics of flow through porous media*. University of Toronto press.
- [19] H. Darcy. (1856). *Les fontaines publiques de la ville de Dijon: exposition et application des principes à suivre et des formules à employer dans les questions de distribution d'eau*. Paris.
- [20] da Silva, M.T.Q.S., do Rocio Cardoso, M., Veronese, C.M.P. & Mazer, W. (2022). Tortuosity: A brief review. *Materials Today: Proceedings*. 58(4), 1344-1349. <https://doi.org/10.1016/j.matpr.2022.02.228>.
- [21] Kadhim, F.S., Samsuri, A. & Kamal, A. (2013). A review in correlations between cementation factor and carbonate rocks properties. *Life Science Journal*. 10(4), 2451-2458.
- [22] Nield, D.A., Bejan, A. (2012). *Convection in porous media*: Springer Fourth edition. <https://doi.org/10.1007/978-1-4614-5541-7>.
- [23] Costa, A. (2006). Permeability-porosity relationship: A reexamination of the Kozeny-Carman equation based on a fractal pore-space geometry assumption. *Geophysical Research Letters*. 33(2), 1-5. <https://doi.org/10.1029/2005GL025134>.
- [24] Slichter, C.S. (1899). *Theoretical investigation of the motion of ground waters*. Geological Survey (U.S.). Ground Water Branch.
- [25] Leibenzon, L.S. (1947). Dvizhenie prirodnykh zhidkosti i gazov v poristoi srede. In *The Motion of Natural Liquids and Gases in a Porous Medium*. Gostekhizdat, Moscow.
- [26] Sundaram, D., Svidró, J.T., Svidró, J. & Diószegi, A. (2021). On the relation between the gas-permeability and the pore characteristics of furan sand. *Materials*. 14(14), 3803, 1-14. <https://doi.org/10.3390/ma14143803>.
- [27] Sundaram, D., Svidró, J.T., Svidró, J. & Diószegi, A. (2022). A novel approach to quantifying the effect of the density of sand cores on their gas permeability. *Jornal of Casting & Materials Engineering*. 6(2), 33-38. <https://doi.org/10.7494/jcme.2022.6.2.33>.
- [28] Costanza-Robinson, M.S. Estabrook, B.D. & Fouhey, D.F. (2011). Representative elementary volume estimation for porosity, moisture saturation, and air-water interfacial areas in unsaturated porous media: Data quality implications. *Water Resources Reserch*. 47(7), 1-12. <https://doi.org/10.1029/2010WR009655>.
- [29] Schindelin, J., Arganda-Carreras, I., Frise, E., Kaynig, V., Longair, M., Pietzsch, T., Preibisch, S., Rueden, C., Saalfeld, S., Schmid, B., Tinevez, J.-Y., White, D.J., Hartenstein, V., Eliceiri, K., Tomancak, P. & Cardona, A. (2012). Fiji: an open-source platform for biological-image analysis. *Nature Methods*. 9, 676-682. <https://doi.org/10.1038/nmeth.2019>.
- [30] Grace, J.R., Ebneyamini, A. (2021). Connecting particle sphericity and circularity. *Particuology*. 54, 1-4. <https://doi.org/10.1016/j.partic.2020.09.006>.
- [31] Vincent, L., Soille, P. (1991). Watersheds in digital spaces: an efficient algorithm based on immersion simulations. *IEEE Transactions on Pattern Analysis & Machine Intelligence*. 13(06), 583-598. <https://doi.org/10.1109/34.87344>.
- [32] Domander, R. Felder, A.A., Doube, M., Schmidt, D. (2021). BoneJ2 - refactoring established research software. *Wellcome Open Research*. 6, 1-21.
- [33] Dougherty, R., Kunzelmann, K.-H. (2007). Computing Local Thickness of 3D Structures with ImageJ. *Microscopy Microanalysis*. 13(S02), 1678-1679. <https://doi.org/10.1017/s1431927607074430>.
- [34] Schmid, B., Schindelin, J., Cardona, A., Longair, M. & Heisenberg, M. (2010). Open Access SOFTWARE A high-level 3D visualization API for Java and ImageJ. *BMC Bioinformatics*. 11, 274, 1-7. <http://www.biomedcentral.com/1471-2105/11/274>.
- [35] Nimmo, J.R. (2004). Porosity and Pore Size Distribution. In Hillel, D.(Eds.), *Encyclopedia of Soils in the Environment*. London, Elsevier,.
- [36] Glover, P.W.J., Walker, E. (2009). Grain-size to effective pore-size transformation derived from electrokinetic theory. *Geophysics*. 74(1), E17-E29. <https://doi.org/10.1190/1.3033217>.
- [37] Graton, L.C. & Fraser, H.J. (1935). Systematic Packing of spheres: with particular relation to porosity and permeability. *The Journal of Geology*. 43(8), 1, 785-909. <http://www.jstor.org/stable/30058420>.
- [38] Holzer, L., Marmet, P., Fingerle, M., Wiegmann, A., Neumann, M., Schmidt, V. (2023). Tortuosity and microstructure effects in porous media. Springer Cham. <https://doi.org/10.1007/978-3-031-30477-4>.